

## Waves for alpha channeling in mirror machines

A. I. Zhmoginov<sup>a)</sup> and N. J. Fisch<sup>b)</sup>

*Department of Astrophysical Sciences, Princeton Plasma Physics Laboratory, Princeton University, Princeton, New Jersey 08543, USA*

(Received 19 June 2009; accepted 28 October 2009; published online 25 November 2009)

Alpha channeling can, in principle, be implemented in mirror machines via exciting weakly damped modes in the ion cyclotron frequency range with perpendicular wavelengths smaller than the alpha-particle gyroradius. Assuming quasilongitudinal or quasitransverse wave propagation, we search systematically for suitable modes in mirror plasmas. Considering two device designs, a proof-of-principle facility and a fusion reactor prototype, we in fact identify candidate modes suitable for alpha channeling. © 2009 American Institute of Physics. [doi:10.1063/1.3265711]

### I. INTRODUCTION

Waves in the ion cyclotron range of frequencies can be employed in magnetic mirror plasmas for plasma production and heating,<sup>1–9</sup> stabilization of plasma instabilities,<sup>10,11</sup> particle injection,<sup>12,13</sup> and plasma diagnostics.<sup>14–17</sup> Alpha channeling is a recently proposed technique<sup>18</sup> for redirecting energy from  $\alpha$  particles to fusion ions by using waves to control the particle dynamics. Originally, the technique was proposed to avoid  $\alpha$  particle damping on waves used in rf current drive techniques,<sup>19</sup> but the waves could also be used to extract energy from the  $\alpha$  particles. In particular, coupling certain rf waves in a tokamak or a mirror machine was predicted<sup>18,20–26</sup> to induce  $\alpha$  particle flows in the phase space leading to quick  $\alpha$  ejection accompanied by  $\alpha$  particle cooling. As a result, the energy with which  $\alpha$  particles are born can be transferred to the waves and then used to sustain fusion reaction in the device. The channeling of the  $\alpha$  power in one simple mirror configuration<sup>27</sup> at ignition has been estimated<sup>24</sup> to increase, potentially, the effective fusion reactivity by a factor of 2.8.

In the absence of external electromagnetic fields, the free energy associated with energetic  $\alpha$  particles can feed numerous plasma instabilities, which can, in turn, transport energy to background plasma species.<sup>28–32</sup> The energy conversion rate in such processes was estimated<sup>29</sup> to be approximately 25%. This suggests that  $\alpha$ -channeling can potentially be a more effective energy transfer mechanism, also capable of fusion ash removal and fuel ion injection.<sup>24,33</sup>

The  $\alpha$ -channeling effect in a mirror machine was shown<sup>24–26</sup> to be possible, in principle, via arranging ion cyclotron wave regions along the device axis (Fig. 1) and adjusting their parameters. In our earlier work,<sup>33</sup> the possibility of the  $\alpha$ -channeling effect in such systems was confirmed numerically by simulating  $\alpha$  particle motion in a magnetic mirror trap. In particular, we offered a preliminary optimization of the device parameters and proposed a prototype configuration capable of extracting 60% of the trapped  $\alpha$  particle energy. However, the restrictions introduced on the wave dispersion by the plasma have not been addressed.

In this work, we analyze the dispersion relation of waves in mirror plasmas and search for the device parameters close to those of the optimum scheme.<sup>33</sup> We consider two different designs of a mirror machine, a proof-of-principle device and a fusion reactor prototype, and identify waves suitable for  $\alpha$ -channeling in both of them. We also show that such waves can be excited at different axial positions if the magnetic field profile has multiple local minima.

The paper is organized as follows. In Sec. II, we use two-dimensional ray-tracing equations to study wave propagation in the central cell of a mirror machine. Assuming that the wave propagates nearly parallel to the magnetic field lines, or in a transverse direction, we simplify equations describing the ray trajectory and propose a method of searching for waves suitable for  $\alpha$ -channeling. In Sec. III, following the approach outlined in Sec. II, we analyze the dispersion relation of plasmas trapped in a mirror machine and search for modes with suitable parameters. After such modes are identified, we simulate ray trajectories numerically to show that the wave packet dynamics is consistent with the analytical predictions and that the identified modes are indeed suitable for  $\alpha$ -channeling. Section IV summarizes our conclusions. In the Appendix, we derive limitations on the wave parameters necessary for efficient  $\alpha$ -channeling.

### II. QUASILONGITUDINAL AND QUASITRANSVERSE WAVE PROPAGATION

As we show in the Appendix, the  $\alpha$ -channeling technique can be implemented in a mirror machine by exciting electromagnetic waves in the ion-cyclotron frequency range with  $k_{\parallel} \ll k_{\perp}$  and  $k_{\perp} \rho_{\alpha} \geq 1$ , such that: (a) they are weakly damped, and (b) the damping on electrons is much weaker compared with the damping on ions. In tokamaks, a leading candidate wave having this property was the mode converted ion Bernstein wave.<sup>34</sup> We now propose a method which can be used to identify waves satisfying these conditions in a mirror device.

#### A. Ray-tracing equations

In this subsection, we write ray-tracing equations in the system of coordinates adjusted to the magnetic field lines. Considering wave propagation outside of the regions of

<sup>a)</sup>Electronic mail: azhmogin@princeton.edu.

<sup>b)</sup>Electronic mail: fisch@princeton.edu.

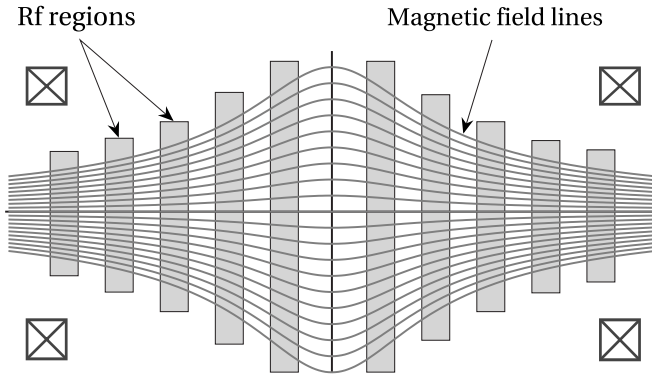


FIG. 1. Arrangement of rf regions (gray bars) in a mirror machine. These regions contain radially and axially localized azimuthally propagating waves in the ion cyclotron frequency range.

strong damping, we assume that the device is large enough to fit many wavelengths so that the geometrical optics approximation is valid. Introducing a characteristic device length  $L$ , and a characteristic device diameter  $d \ll L$ , this condition can be rewritten as  $k_{\parallel}L \gg 1$  and  $k_{\perp}d \gg 1$ . Fixing the azimuthal wave number  $m$ , the two-dimensional ray trajectory  $\mathbf{r}(t)$ ,  $\mathbf{k}(t)$  can be obtained as a solution of the system<sup>35</sup>

$$\frac{d\mathbf{r}}{d\tau} = \frac{\partial \mathcal{D}}{\partial \mathbf{k}}, \quad \frac{d\mathbf{k}}{d\tau} = -\frac{\partial \mathcal{D}}{\partial \mathbf{r}}, \quad (1)$$

where  $\mathcal{D}=0$  is a wave dispersion relation,  $\mathbf{r}=(r, z)$  and  $\mathbf{k}=(k_r, k_z)$  are the two-dimensional wave packet position and wave vectors correspondingly, and  $\tau$  is the new independent variable, or “time” defined through

$$\frac{dt}{d\tau} = \frac{\partial \mathcal{D}}{\partial \omega}. \quad (2)$$

Consider  $\mathcal{D}$  as a function of  $k_{\parallel}=\mathbf{k} \cdot \hat{\mathbf{b}}$  and  $k_n=\mathbf{k} \cdot \hat{\mathbf{n}}$ , where  $\hat{\mathbf{b}}$  is a two-dimensional unit vector directed along the magnetic field and  $\hat{\mathbf{n}}$  is a two-dimensional unit vector perpendicular to  $\hat{\mathbf{b}}$  such that  $n_r > 0$ ; then one can rewrite the ray-tracing equations as

$$\dot{r} = \frac{\partial \mathcal{D}}{\partial k_{\parallel}} \hat{b}_r + \frac{\partial \mathcal{D}}{\partial k_n} \hat{b}_z, \quad (3)$$

$$\dot{z} = \frac{\partial \mathcal{D}}{\partial k_{\parallel}} \hat{b}_z - \frac{\partial \mathcal{D}}{\partial k_n} \hat{b}_r, \quad (4)$$

$$\dot{k}_{\parallel} = -\hat{b}_r \left. \frac{\partial \mathcal{D}}{\partial r} \right|_{k_{\parallel}, k_n} - \hat{b}_z \left. \frac{\partial \mathcal{D}}{\partial z} \right|_{k_{\parallel}, k_n} + \frac{\partial \mathcal{D}}{\partial k_n} \left[ \frac{k_{\parallel}}{\rho_{\parallel}} + \frac{k_n}{\rho_{\perp}} \right], \quad (5)$$

$$\dot{k}_n = -\hat{b}_z \left. \frac{\partial \mathcal{D}}{\partial r} \right|_{k_{\parallel}, k_n} + \hat{b}_r \left. \frac{\partial \mathcal{D}}{\partial z} \right|_{k_{\parallel}, k_n} - \frac{\partial \mathcal{D}}{\partial k_{\parallel}} \left[ \frac{k_{\parallel}}{\rho_{\parallel}} + \frac{k_n}{\rho_{\perp}} \right], \quad (6)$$

where  $\rho_{\parallel}^{-1} = \hat{\mathbf{n}} \cdot [(\hat{\mathbf{b}} \nabla) \hat{\mathbf{b}}]$  is the magnetic field curvature, and  $\rho_{\perp}^{-1} = \hat{\mathbf{n}} \cdot [(\hat{\mathbf{n}} \nabla) \hat{\mathbf{b}}]$  is the curvature of lines in  $(r, z)$  plane transverse to the magnetic field lines. For convenience, we will further work in the system of coordinates adjusted to the magnetic field lines. In particular, instead of defining the

wave packet position  $(r, z)$  in cylindrical coordinates, we will characterize its position by a tuple  $(R, \eta)$ , where  $R \approx r \sqrt{B(\eta)/B_0}$  is a midplane distance from the system axis to the field line on which the wave packet resides,  $B_0 = B(0)$  is a midplane magnetic field and  $\eta$  is a coordinate along the field line such that  $\eta=0$  on the midplane and  $d\eta = \hat{b}_z dz + \hat{b}_r dr$ .

## B. Quasilonitudinal propagation

Assume that the group velocity of the wave packet is directed primarily along the magnetic field and that the radial gradients can be neglected. This makes negligible the term  $-\partial \mathcal{D} / \partial n \equiv -\hat{b}_z \partial \mathcal{D} / \partial r + \hat{b}_r \partial \mathcal{D} / \partial z$  in Eq. (6). In this case, the ray trajectory describes wave packets quickly moving along the magnetic field lines, while drifting slowly in  $R$ . Since  $R \ll L$ , the term proportional to  $\rho_{\parallel}^{-1}$  can be neglected compared with  $\rho_{\perp}^{-1}$ . Substituting  $\rho_{\perp}^{-1} \approx -(2B)^{-1} dB / d\eta$  in Eq. (6), one then obtains  $k_n = \zeta \sqrt{B}$ , where  $\zeta$  is a constant. As a result, the longitudinal wave packet motion can be described by the Hamiltonian

$$H(k_{\parallel}, \eta; \zeta, R) = \mathcal{D}(k_{\parallel}, k_n = \zeta \sqrt{B(\eta)}, \eta, R) = 0,$$

where  $k_{\parallel}$  is a canonical momentum,  $\eta$  is a canonical coordinate, and  $\zeta, R$  are slowly changing parameters. To find how the  $k_{\parallel}(\eta)$  dependence evolves with time, note that since motion in  $(k_{\parallel}, \eta)$  space is fast compared with the transverse motion, the adiabatic invariant  $I_{\parallel} = \oint k_{\parallel} d\eta$  must be approximately conserved. This property and the knowledge of the slowly changing  $\zeta$  and  $R$  defines  $k_{\parallel}(\eta)$ . The evolution of  $\zeta$  and  $R$  can be calculated either using the following averaged equations:

$$\dot{\zeta} = - \left\langle \frac{1}{\sqrt{B}} \frac{\partial \mathcal{D}}{\partial n} \right\rangle, \quad \dot{R} = \left\langle \sqrt{B} \frac{\partial \mathcal{D}}{\partial k_n} \right\rangle,$$

where the averaging is performed over the fast longitudinal oscillations, or using the conservation of  $I_{\parallel}$  which restricts motion in  $(\eta, R)$  to a one-dimensional curve. A more strict derivation of these equations will be discussed in our future work.

If, for a wave of interest,  $k_{\parallel} \ll k_n$  and  $\eta \ll L$ , one can decompose

$$\mathcal{D} \approx \mathcal{D}_0(k_n, R) + \alpha(k_n, R) k_{\parallel}^2 / 2 + \beta(k_n, R) \eta^{2g} / 2g, \quad (7)$$

where  $g$  is some integer number. Therefore, neglecting first order corrections with respect to  $k_{\parallel}$  and  $\eta$ , averaged motion in  $k_n$  and  $R$  satisfies  $\mathcal{D}_0(k_n, R) \approx 0$ . Substituting this solution in the expressions for  $\alpha(k_n, R)$  and  $\beta(k_n, R)$ , we can describe the shape of the longitudinal ray trajectory in  $(k_{\parallel}, \eta)$  space as the wave packet slowly drifts radially in the device.

The  $\alpha$ -channeling technique is practical if the energy extracted from  $\alpha$  particles exceeds the energy necessary to excite the channeling wave (see Appendix, Sec. 3). Under the realistic assumption that the  $\alpha$  particle birth rate is not so large that the catalytic wave energy can be significantly amplified in a single longitudinal pass through the central cell, it follows that the catalytic wave should be a weakly damped mode trapped in the device core. Such modes can be identi-

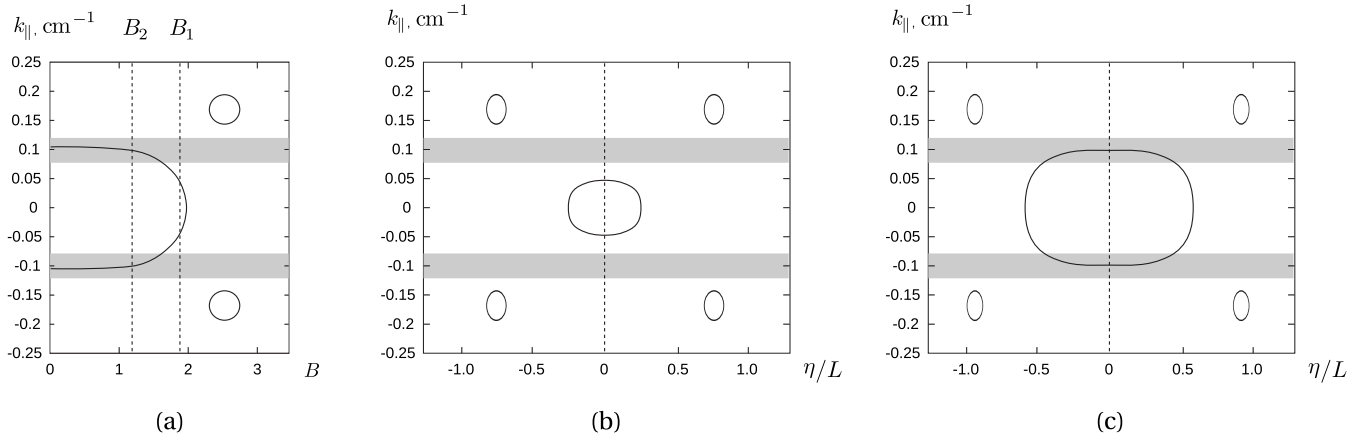


FIG. 2. A conceptual plot of  $k_{\parallel}(B)$  and  $k_{\parallel}(\eta)$  dependencies plotted for different values of the midplane magnetic field  $B_0$ : (a) the original  $k_{\parallel}(B)$  dependence showing two closed loops and a half of a loop located in the vicinity of  $B=B_1$  (gray bars indicate areas of strong wave damping), (b)  $k_{\parallel}(\eta)$  dependence plotted for the mirror machine with  $B_0=B_1$ , (c)  $k_{\parallel}(\eta)$  dependence plotted for  $B_0=B_2$ . The choice of  $B_0=B_1$  results in a weakly damped mode trapped in the device core, while in  $B_0=B_2$  case, the corresponding wave is strongly damped.

fied as closed loops on the graph  $k_{\parallel}(\eta; \zeta, R)$ , which also avoid regions of strong electron and ion Landau damping ( $\omega/k_{\parallel} \sim w_{ei}$ ) and regions of strong ion cyclotron damping [ $(\omega - n\Omega_i)/k_{\parallel} \sim w_i$ ], where  $w_s$  is a thermal velocity of the species  $s$ . We will denote such loops as *candidate loops*. The value of  $k_{\parallel}$  solving  $H(k_{\parallel}, \eta; \zeta, R) = 0$  depends on  $\eta$  through the longitudinal plasma parameter profiles. Neglecting effects associated with the longitudinal plasma temperature variation, and assuming that the line plasma density is nearly constant along a field line and hence  $n(\eta) \approx n_0 B(\eta)/B_0$ , one can express the longitudinal wave number as  $k_{\parallel}(B(\eta); \omega, m, \zeta, R\sqrt{B_0}, n_0/B_0, T_{ei})$ . One can then plot  $k_{\parallel}(B)$  for fixed parameter values, and search for value for  $B_0$  and the mirror ratio  $R_B$  such that there is a loop on the  $k_{\parallel}(\eta)$  graph. Plotted as a function of  $B$ , such a loop can be located either in the middle of the segment  $[B_0, R_B B_0]$  or be “wrapped” around one of its ends, in which case the  $k_{\parallel}(B)$  graph, restricted to  $B_0 \leq B \leq R_B B_0$ , shows just a half loop (see Fig. 2). In conclusion, in order to find a system which allows for a slowly damped longitudinally propagating wave trapped in it, one needs to study  $k_{\parallel}(B)$  dependencies plotted for different values of  $\omega$ ,  $m$ ,  $\zeta$ ,  $n/B$ ,  $r\sqrt{B}$ , and  $T$ . The features indicating the existence of the mode include either the presence of the candidate loop, or a half loop, located at  $B=B_0$ , or at  $B=R_B B_0$  for some  $B_0$  and  $R_B$ .

### C. Quasitransverse propagation

Assume now that the wave of interest is instead propagating nearly perpendicular to the magnetic field lines. Since we suppose that the motion in  $(k_n, R)$  variables is fast, while the quiver motion in  $(k_{\parallel}, \eta)$  is negligible, the wave packet averaged motion along the magnetic field line can be described by

$$\dot{\eta} \approx \left\langle \frac{\partial D}{\partial k_{\parallel}} \right\rangle, \quad (8)$$

$$\dot{k}_{\parallel} \approx - \left\langle \frac{\partial \mathcal{D}_0}{\partial \eta} \right\rangle + \left\langle k_n \frac{\partial \mathcal{D}_0}{\partial k_n} \right\rangle \frac{1}{\rho_{\perp}}, \quad (9)$$

where the averaging is performed over oscillations in  $(k_n, R)$  space. The quiver motion in  $(k_n, R)$  variables can be found independently using an approximate local dispersion relation  $\mathcal{D}(k_n, R; k_{\parallel}, \eta) = 0$  and  $\dot{R} = \partial \mathcal{D} / \partial k_n$ . Note that the slow motion in  $(k_{\parallel}, \eta)$  can also be found from the conservation of the adiabatic invariant  $I_{\perp}(k_{\parallel}, \eta) = \oint k_n(R; k_{\parallel}, \eta) dR$  associated with the fast oscillations.

To simplify Eqs. (8) and (9), assume further that  $k_{\parallel} \ll k_n$ , and that the transversely propagating wave is localized near the midplane at  $\eta \ll L$ . Decomposing again  $\mathcal{D} \approx \mathcal{D}_0(k_n, R) + \alpha(k_n, R)k_{\parallel}^2/2 + \beta(k_n, R)\eta^{2g}/2g$ , one approximates

$$\dot{\eta} \approx \langle \alpha \rangle k_{\parallel}, \quad (10)$$

$$\dot{k}_{\parallel} \approx - \langle \beta \rangle \eta^{2g-1} + g \left\langle \frac{\partial \mathcal{D}_0}{\partial k_n} k_n \right\rangle \frac{\eta^{2g-1}}{L^{2g}} = - \gamma \eta^{2g-1}. \quad (11)$$

If  $\langle \alpha \rangle \gamma > 0$ , Eqs. (10) and (11) describe the particle motion in the attractive potential  $U(\eta) = \langle \alpha \rangle \gamma \eta^{2g}$ . Hence, the corresponding ray trajectories will be bounded in  $(k_{\parallel}, \eta)$ , and under a proper choice of initial parameters they will be weakly damped on electrons due to  $k_{\parallel} \ll \omega/w_e$ . To identify such waves, one needs to study  $k_{\parallel}(B)$  dependencies and look for waves with  $k_{\parallel} \approx 0$ . If  $\langle \alpha \rangle \gamma > 0$ , and the transverse motion of the found wave is quick compared with the longitudinal motion, then the ray trajectory evolution in  $(k_{\parallel}, \eta)$  space satisfies Eqs. (10) and (11), and such a wave can be suitable for  $\alpha$ -channeling.

### III. NUMERICAL SIMULATIONS

To illustrate the methods discussed in Sec. II and to show that weakly damped modes can exist in practical fusion devices, we consider two mirror machine designs: a proof-of-principle facility and a fusion reactor prototype with pa-

rameters similar to those used in Refs. 36 and 37. We assume that the magnetic field  $\mathbf{B}$  in both devices is given by  $B_\phi=0$ ,  $B_r=-r(dB_z/dz)/2$ , and

$$B_z = B_{\min} + \frac{1}{2}(B_{\max} - B_{\min})[1 - \cos(\pi|2\eta z/L|^g)],$$

where  $g$  is an integer,  $\eta \geq 1$  is a constant,  $B_{\min}$  and  $B_{\max}$  are the minimum and the maximum values of  $B_z$  correspondingly. We also assume that (i) the linear density of the plasma does not depend on the axial position, and hence  $n(z)|_{R=0} \approx n^0 B(z)/B_0$  on the axis, and (ii) that radial plasma temperature and density profiles are given by  $n(r, z) = n(z)|_{R=0} \exp(-R^2/a^2)$  and  $T(r) = T^0[\kappa + (1 - \alpha)\exp(-R^2/a^2)]$ , where  $\alpha \leq 1$  is a constant, and  $a$  is a characteristic plasma radius. The dispersion relation  $\mathcal{D}=0$  is modeled by the plasma kinetic dispersion relation reading  $\mathcal{D} = \|\hat{\epsilon} - n^2 \hat{\mathbf{1}} + \mathbf{nn}\|$ , where  $\hat{\epsilon} = \hat{\mathbf{1}} + \sum_s \hat{\chi}_s$ ,  $\hat{\chi}_s = \omega_{ps}^2 / \omega \cdot \sum_n e^{-\lambda} \hat{Y}_n^s(\lambda)$ , and tensor  $\hat{Y}_n^s(\lambda)$  is given by the following expression:<sup>35</sup>

$$\hat{Y}_n^s = \begin{pmatrix} \frac{n^2 I_n A_n}{\lambda_s} & -in \Delta I_n A_n & \frac{k_\perp n I_n B_n}{\Omega_s \lambda_s} \\ in \Delta I_n A_n & Q A_n & \frac{ik_\perp \Delta I_n B_n}{\Omega_s} \\ \frac{k_\perp n I_n B_n}{\Omega_s \lambda_s} & -\frac{ik_\perp \Delta I_n B_n}{\Omega_s} & \frac{2(\omega - n\Omega_s)}{k_\parallel w_{s\perp}^2} I_n B_n \end{pmatrix}.$$

Here  $\omega_{ps}^2$  is the plasma frequency for species  $s$ ,  $Q = (n^2 I_n \lambda_s^{-1} + 2\lambda_s \Delta I_n)$ ,  $\Delta I_n = I_n(\lambda_s) - I_n'(\lambda_s)$ ,  $A_n = (k_\parallel w_{s\parallel})^{-1} Z_0(\xi_n^s)$ ,  $B_n = k_\perp^{-1} [1 + \xi_n^s Z_0(\xi_n^s)]$ ,  $\xi_n^s = (\omega - n\Omega_s)(k_\parallel w_{s\parallel})^{-1}$ ,  $\lambda_s = k_\perp^2 \rho_s^2 / 2$ ,  $Z_0$  is the real part of the plasma dispersion function,  $w_{s\parallel}$  and  $w_{s\perp}$  are parallel and perpendicular thermal particle velocities correspondingly,  $\rho_s = w_{s\perp} / \Omega_s$ , and  $\Omega_s$  is the gyrofrequency.

### A. The function $k_\parallel(\mathbf{B})$ for the proof-of-principle facility

For a proof-of-principle facility<sup>36,37</sup> consider an open system with characteristic diameter  $d=6a=1.2$  m, central cell length  $L=12$  m, ion and electron temperatures on the axis  $T_e^0 = T_i^0 = 4$  keV,  $\kappa=0.15$ ,  $B \sim 1$  T, and electron and ion densities on axis at the midplane  $n_e^0 = n_D^0 + n_T^0$  being of order of  $10^{13}$  cm<sup>-3</sup> with  $n_D^0$  and  $n_T^0$  being the deuterium and tritium densities correspondingly.

Consider first the case  $k_\perp \rho_\alpha \sim 1$ , which implies  $k_\perp \rho_i \ll 1$ . Calculating the dependence  $k_\parallel(B)$  numerically for  $r\sqrt{B} = 18.3$  cm  $\times$  T<sup>1/2</sup>,  $n_D^0/n_T^0 = 1$ ,  $n/B = 6.67 \times 10^{12}$  cm<sup>-3</sup> T<sup>-1</sup>,  $m=1$ ,  $\zeta = 0.045$  cm<sup>-1</sup> T<sup>-1/2</sup>, and  $\omega \approx 5.8 \times 10^7$  s<sup>-1</sup> approximately equal to the deuterium gyrofrequency in the magnetic field  $B_\omega = 1.2$  T, several loop candidates were identified (Fig. 3). Both parts of the plot indicated by circles lie outside of the areas susceptible to strong Landau and ion cyclotron damping and have reflection points at the higher values of the magnetic field. Hence, both of these curve segments described by an approximate dispersion relation

$$a = n_\parallel^2 + \frac{d^2}{b - n^2}, \quad (12)$$

where

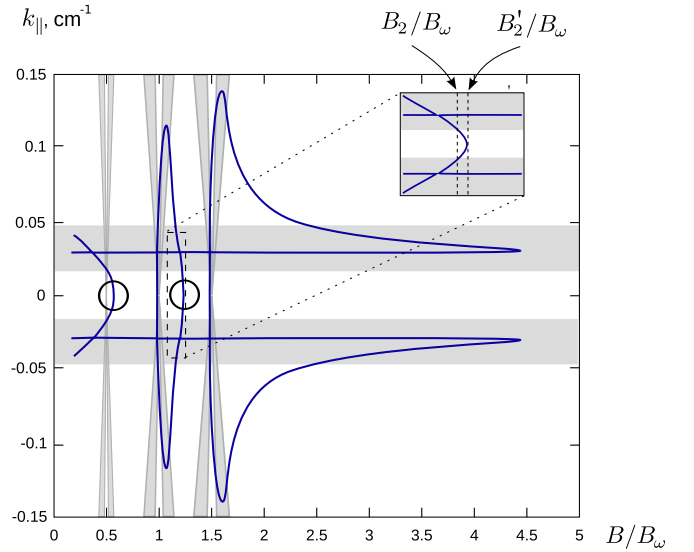


FIG. 3. (Color online) Dependence of  $k_\parallel$  on  $B/B_\omega$  for  $\omega \approx 5.8 \times 10^7$  s<sup>-1</sup>,  $r\sqrt{B} = 18.3$  cm  $\times$  T<sup>1/2</sup>,  $n_D^0/n_T^0 = 1$ ,  $n/B = 6.67 \times 10^{12}$  cm<sup>-3</sup> T<sup>-1</sup>,  $m=1$ , and  $\zeta = 0.045$  cm<sup>-1</sup> T<sup>-1/2</sup>. Parts of the dispersion curve lying inside the gray areas correspond to waves strongly damped through electron Landau resonance, or ion cyclotron resonance. Circles indicate the parts of the dispersion curve in the regions  $[B_{1/2}/B_\omega, B'_{1/2}/B_\omega]$  corresponding to the weakly damped mode candidates. The inset shows zoomed in band  $[B_2/B_\omega, B'_2/B_\omega]$  in better resolution.

$$a \approx 1 - \sum_i \frac{\omega_{pi}^2}{\omega} \sum_n e^{-\lambda_i} \frac{n^2 I_n(\lambda_i)}{\lambda_i (\omega - n\Omega_i)},$$

$$b \approx 1 - \sum_i \frac{\omega_{pi}^2}{\omega} \sum_n \frac{e^{-\lambda_i}}{\omega - n\Omega_i} \left[ \frac{n^2 I_n(\lambda_i)}{\lambda_i} + 2\lambda_i (I_n - I_n') \right],$$

$$d \approx \sum_i \frac{\omega_{pi}^2}{\omega} \sum_n \frac{ne^{-\lambda_i} (I_n - I_n')}{\omega - n\Omega_i} + \frac{\omega_{pe}^2}{\omega \Omega_e},$$

might correspond to weakly damped modes trapped near the midplane. This dispersion relation was derived from  $\|\hat{\epsilon} - n^2 \hat{\mathbf{1}} + \mathbf{nn}\| = 0$  neglecting  $n_\perp^2$  compared with  $\epsilon_{zz}$ , neglecting  $\epsilon_{xz}$ ,  $\epsilon_{zx}$ ,  $\epsilon_{xy}$ ,  $\epsilon_{yx}$ , and assuming that  $\Omega_e \gg \omega$ . The dispersion relation (12) is the finite- $k_\perp \rho$  version of the fast wave dispersion relation for cold plasmas obeying  $(S - n_\parallel^2)(S - n^2) = D^2$ , where

$$S = 1 + \sum_s \frac{\omega_{ps}^2}{\Omega_s^2 - \omega^2},$$

$$D = \sum_s \frac{\omega_{ps}^2 \Omega_i}{\omega (\Omega_s^2 - \omega^2)}.$$

However, while Eq. (12) describes both of the predicted waves with  $k_\parallel \approx 0$  shown in Fig. 3, the cold plasma dispersion relation holds only at  $\omega \approx \Omega_D$ .

Notice that for both loop candidates shown in Fig. 3,  $k_\parallel \ll k_n$ . Note also that these candidates exist in the local minimum of the magnetic field only. Numerical calculations of  $k_\parallel(B)$  for other wave and plasma parameters (different from those used in Fig. 3 by no more than one order of magnitude) did not reveal any candidate waves which either

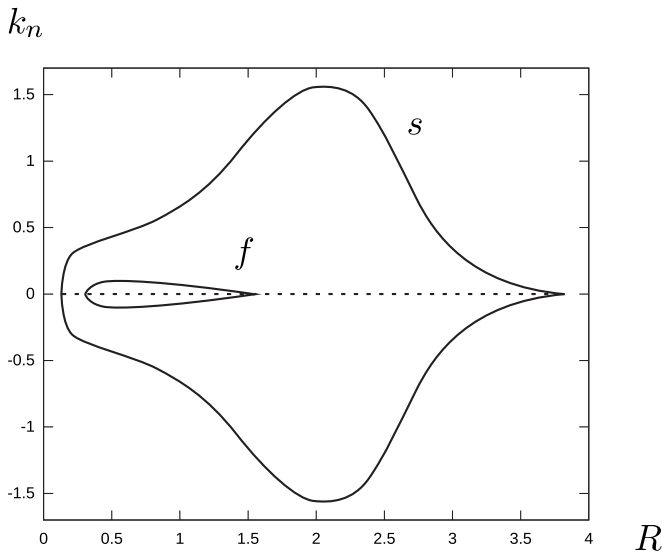


FIG. 4. Solution of equation  $\mathcal{D}_0(k_n, R) = 0$  for  $\omega \approx 5.8 \times 10^7 \text{ s}^{-1}$ ,  $T_e^0 = T_i^0 = 4 \text{ keV}$ ,  $n_e^0 \approx 7.4 \times 10^{12} \text{ cm}^{-3}$ ,  $\kappa = 0.15$ ,  $n_D^0/n_T^0 = 1$ ,  $m = 1$ , and  $B \approx 1.5 \text{ T}$ . The slow trajectory, period of motion along which is much larger than the characteristic period of the longitudinal oscillations, is marked with letter *s*. The fast trajectory is marked with letter *f*. The period of oscillations along this trajectory is much smaller than the characteristic period of the longitudinal motion.

had  $k_{\parallel} \geq k_n$ , or were represented by closed loops in  $k_{\parallel}(B)$  plot. Hence, for  $k_{\perp} \rho_i \ll 1$ , the observed candidate waves can be studied assuming quasilonitudinal, or quasitransverse propagation and using Eq. (7). Furthermore, numerically calculating  $k_{\parallel}(B)$  for  $k_{\perp} \rho_i \geq 1$  for plasma and wave parameters similar to those used in the  $k_{\perp} \rho_i \ll 1$  case, we also did not observe candidate waves with  $k_{\parallel} \geq k_n$ , or closed loops in the  $k_{\parallel}(B)$  plot. This suggests that the candidate waves with  $k_{\perp} \rho_i \geq 1$  can be studied using the same approach used for the waves with  $k_{\perp} \rho_i \ll 1$ .

## B. Quasilonitudinal and quasitransverse waves in the proof-of-principle facility

We now study wave candidates similar to those shown in Fig. 3. We assume that the corresponding waves propagate either quasilonitudinally or quasitransversely and that for such waves  $k_{\parallel} \ll k_n$  and  $\eta \ll L$ . Using Eq. (7), one obtains approximate expression for the wave packet trajectory in  $(k_n, R)$  space

$$\mathcal{D}_0(k_n, R) \approx 0.$$

The numerical solution of this equation for  $\omega \approx 5.8 \times 10^7 \text{ s}^{-1}$ ,  $T_e^0 = T_i^0 = 4 \text{ keV}$ ,  $n_e^0 \approx 7.4 \times 10^{12} \text{ cm}^{-3}$ ,  $n_D^0/n_T^0 = 1$ ,  $\kappa = 0.15$ ,  $m = 1$ , and  $B \approx 1.5 \text{ T}$  is shown on Fig. 4. According to this figure, there are two distinct trajectories in  $(k_n, R)$  space, for one of which, marked with “*s*,” the characteristic period of motion  $T_s$  is of order of  $10T_l$ , while for another, marked with “*f*,” the period of motion  $T_f$  is of order of  $0.02T_l$ . Here  $T_l$  is a characteristic period of the longitudinal motion calculated for the ray trajectory with  $k_{\parallel} \sim 0.004 \text{ cm}^{-1}$ . Since  $T_f \ll T_l \ll T_s$ , the trajectory marked with *s* corresponds to the longitudinal wave propagation, while the trajectory marked with *f* corresponds to the transverse case. An example of a ray trajectory plotted for the longitudinal case is shown on Fig. 5. According to this figure, which captures one period of slow motion in  $(k_n, R)$ , the parallel adiabatic invariant  $I_{\parallel}$  is nearly conserved. Due to  $I_{\parallel}$  conservation, the maximum value of  $k_{\parallel}$  is reached near the point of the curve  $\mathcal{D}_0(k_n, R) = 0$ , where  $\beta/\alpha$  reaches maximum. For the parameters used to plot Fig. 5, the minimum of  $v_{\text{ph}}/w_e = \omega/(k_{\parallel}w_e)$  is approximately equal to 3 and, therefore, the corresponding wave is weakly damped on electrons.

For the transversely propagating wave, there exist two possible regimes. In one of them, shown in Fig. 6 with a dashed line, the characteristic reflection time, on which  $k_{\parallel}$  changes sign, is of order of  $T_f$ . In this regime, the description

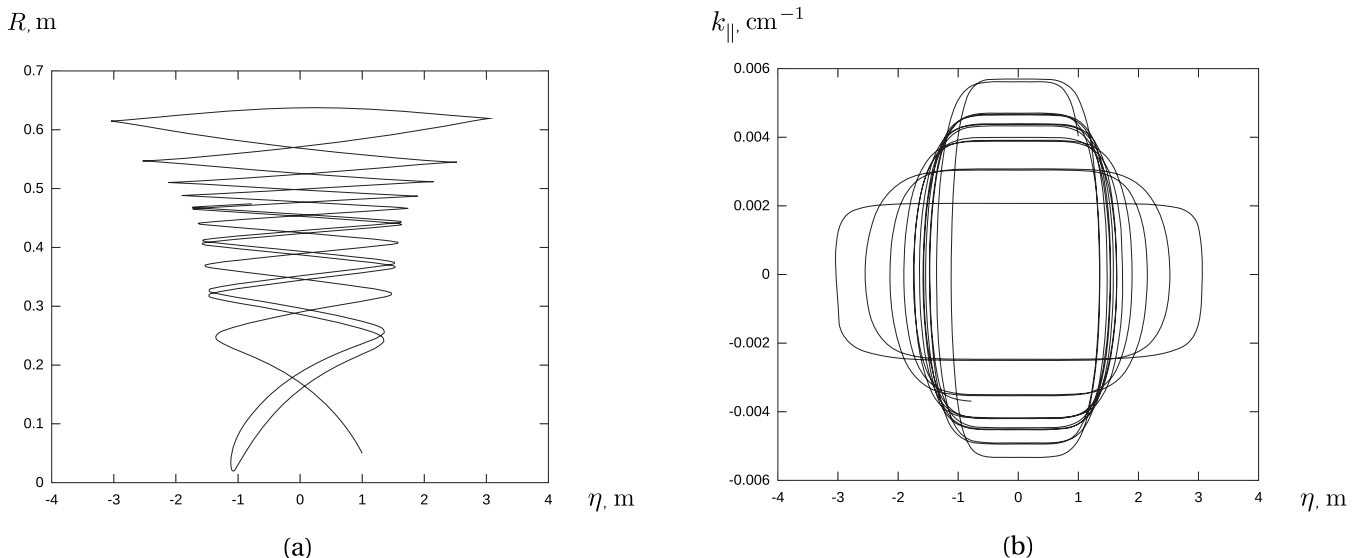


FIG. 5. Ray trajectory plotted for the longitudinally propagating wave: (a) ray trajectory in  $(k_{\parallel}, \eta)$  space, (b) ray trajectory in  $(r, z)$  coordinates. The system parameters are  $\omega \approx 5.8 \times 10^7 \text{ s}^{-1}$ ,  $T_e^0 = T_i^0 = 4 \text{ keV}$ ,  $n_e^0 \approx 7.4 \times 10^{12} \text{ cm}^{-3}$ ,  $n_D^0/n_T^0 = 1$ ,  $\kappa = 0.15$ ,  $m = 1$ ,  $B_{\text{min}} \approx 1.5 \text{ T}$ , and  $B_{\text{max}} = 5B_{\text{min}}$ . The ray is launched from the point with  $k_{\parallel}^0 = 0.004 \text{ cm}^{-1}$  and  $\eta = 1 \text{ m}$ .

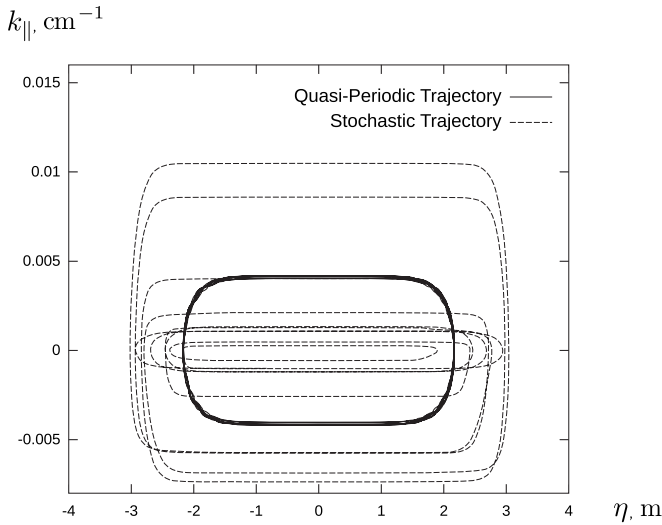


FIG. 6. Ray trajectories in  $(k_{\parallel}, \eta)$  space for two quasitransverse waves: (i) chaotic trajectory plotted for the case  $T_f \sim T_r$  (dashed), where  $T_r$  is a characteristic  $k_{\parallel}$  reflection time and (ii) quasiperiodic trajectory for  $T_f \ll T_r$  (solid). Both trajectories are simulated for the system with  $\omega \approx 5.8 \times 10^7 \text{ s}^{-1}$ ,  $m=1$ ,  $\kappa=0.15$ ,  $n_e^0 \approx 9.8 \times 10^{12} \text{ cm}^{-3}$ ,  $B_{\min} \approx 1.5 \text{ T}$ , and  $B_{\max} = 5B_{\min}$ . The random walk occurs in a system with  $T_e^0 = T_i^0 = 4 \text{ keV}$  and  $n_T/n_D=1$ , while the quasiperiodic trajectory is plotted for the case  $T_e^0 = T_i^0 = 2 \text{ keV}$  and  $n_T/n_D=1.5$ .

of the longitudinal motion by particle motion in the potential  $U(\eta) = \langle \alpha \rangle \gamma \eta^{2s}$  is inaccurate. Instead, there will be a random walk in  $k_{\parallel}$  as a result of which a wave packet can approach  $k_{\parallel} \sim \omega/w_e$  and become strongly damped on electrons. In another regime shown in Fig. 6 with a solid line, the characteristic reflection time is much larger than  $T_f$ . In this case, the ray trajectory can be described by the equations of motion in the potential  $U(\eta) = \langle \alpha \rangle \gamma \eta^{2s}$  and as a result, such wave can remain weakly damped after many longitudinal oscillations.

To provide examples of the modes weakly damped on electrons, but interacting with deeply trapped  $\alpha$  particles, we considered several system designs. The best result for the  $k_{\perp} \rho_i \ll 1$  case was achieved for the system with  $\omega \approx 5.8 \times 10^7 \text{ s}^{-1}$ ,  $T_e^0 = T_i^0 = 4 \text{ keV}$ ,  $n_e^0 \approx 4.2 \times 10^{12} \text{ cm}^{-3}$ ,  $n_D^0/n_T^0=1$ ,  $m=1$ , and  $B \approx 0.6 \text{ T}$ . In this configuration,  $\omega \approx 2\Omega_D$  and the interaction with  $\alpha$  particles occurs through the second cyclotron resonance. The quasitransverse wave launched near the midplane at  $R=20 \text{ cm}$  and having initial  $k_{\parallel} \sim 0.005 \text{ cm}^{-1}$  was shown to be weakly damped on electrons since  $\min v_{\text{ph}}/w_e \approx 3.5$  and strongly interacting with  $\alpha$  particles because  $\min v_{\text{res}}/w_{\alpha} \approx 0.34$ , where  $v_{\text{res}}$  is a resonance parallel velocity calculated for  $n=2$ . The mode was also shown to be bounded radially and longitudinally in a region with  $\Delta R \sim 30 \text{ cm}$  and  $\Delta \eta \sim 4 \text{ m}$ .

This mode was found using the geometrical optics approximation. However, it may exist even when the approximation fails. Even though the characteristic values of  $k_n \Delta R$  and  $k_{\parallel} \Delta \eta$  were approximately equal to 2.5, and hence, the conditions of applicability of the geometrical optics approximation were not satisfied, one can still expect that a similar wave with a frequency close to that given by the Wentzel–Kramers–Brillouin quantization condition can, in principle, be excited in a device of similar size. A full wave simulation

would be, of course, necessary to find the corresponding mode frequency as well as the mode structure. Interestingly, both  $k_n \Delta R$  and  $k_{\parallel} \Delta \eta$  can be increased for fixed device scale sizes and fixed  $B_0$  by considering higher-order cyclotron resonances. Numerical simulations confirmed that after doubling  $\omega$  (so that  $\omega \approx 4\Omega_D$ ), not only can the characteristic  $k_{\parallel}$  be doubled while leaving  $\omega/(k_{\parallel} w_e)$  the same as for  $\omega \approx 2\Omega_D$ , but the maximum  $k_n$  achieved for the quasitransverse wave is also nearly doubled. As a result,  $k_n \Delta R$  increased nearly three times (due to both  $k_n$  and  $\Delta R$  increase), while  $k_{\parallel} \Delta \eta$  increased more than twice.

For the  $k_{\perp} \rho_i \gg 1$  case, we considered quasilongitudinal modes in the system with  $\omega \approx 5.8 \times 10^7 \text{ s}^{-1}$ ,  $T_e^0 = T_i^0 = 4 \text{ keV}$ ,  $n_e^0 \approx 7.6 \times 10^{12} \text{ cm}^{-3}$ ,  $n_D^0/n_T^0=1$ ,  $m=20$ , and  $B \approx 1.15 \text{ T}$ . The wave was launched close to the device periphery at  $R=55 \text{ cm}$  with initial  $k_{\parallel} \sim 0.006 \text{ cm}^{-1}$  and was shown to be weakly damped on electrons (since  $\min v_{\text{ph}}/w_e \approx 3.5$ ) and strongly interacting with  $\alpha$  particles (since  $\min v_{\text{res}}/w_{\alpha} \approx 0.42$ ). The mode was bounded both radially with  $\Delta R \sim 60 \text{ cm}$  and longitudinally with  $\Delta \eta \sim 6 \text{ m}$ . Since  $k_n$  reaches 15.0 along the ray trajectory, the radial wave number of the mode is very large and  $\max k_{\perp} \rho_{\alpha} \approx 300$ . The characteristic value  $k_{\parallel} \Delta \eta$ , in turn, was approximately equal to 4 and hence, such a mode can in principle, be excited in the proof-of-principle device.

As an intermediate conclusion, two qualitatively different weakly damped modes with  $k_{\perp} \rho_D \ll 1$  and  $k_{\perp} \rho_D \gg 1$  with  $\tau_i \gg \tau_e$ , capable of resonant interaction with deeply trapped  $\alpha$  particles, have been identified.

### C. Fusion reactor prototype

For a fusion reactor prototype, following Ref. 36, we consider a mirror machine with the following parameters:  $d=6 \text{ m}$ ,  $L=15 \text{ m}$ ,  $B_0=3 \text{ T}$ ,  $n_e^0 = n_D^0 + n_T^0 \approx 10^{14} \text{ cm}^{-3}$ ,  $T_e=60 \text{ keV}$ , and  $T_i=15 \text{ keV}$ . Even though  $w_e \approx 0.2c$ , we neglected relativistic effects and used the same dispersion relation as in Sec. III A. Similarly to the proof-of-principle facility, the dependencies of  $k_{\parallel}$  on  $B$  did not show any candidate waves which either had  $k_{\parallel} \geq k_n$ , or were represented by closed loops on  $k_{\parallel}(B)$  plot. Numerical simulations confirmed that, by analogy with the proof-of-principle facility, in the prototype device, two weakly damped modes capable of resonant interaction with deeply trapped  $\alpha$  particles,  $\tau_i \gg \tau_e$ , and either  $k_{\perp} \rho_D \ll 1$  (quasitransverse wave), or  $k_{\perp} \rho_D \gg 1$  (quasilongitudinal wave) could be identified. However, since in the fusion reactor prototype,  $\omega L/w_e$  is 1.3 times smaller compared with the proof-of-principle facility, we used higher ion cyclotron resonances to satisfy both  $k_{\parallel} \Delta \eta \geq \pi$  and  $k_n \Delta R \geq \pi$ .

### D. Multiple wave regions

The system of rf regions with high  $\alpha$ -channeling efficiency, proposed in Refs. 24 and 25, consisted of several waves located at different axial positions. Unfortunately, the weakly damped mode described by the dispersion relation (12) was shown to exist only in a small vicinity of the local magnetic field minimum and hence could not be employed anywhere except at the midplane. In order to use the mode

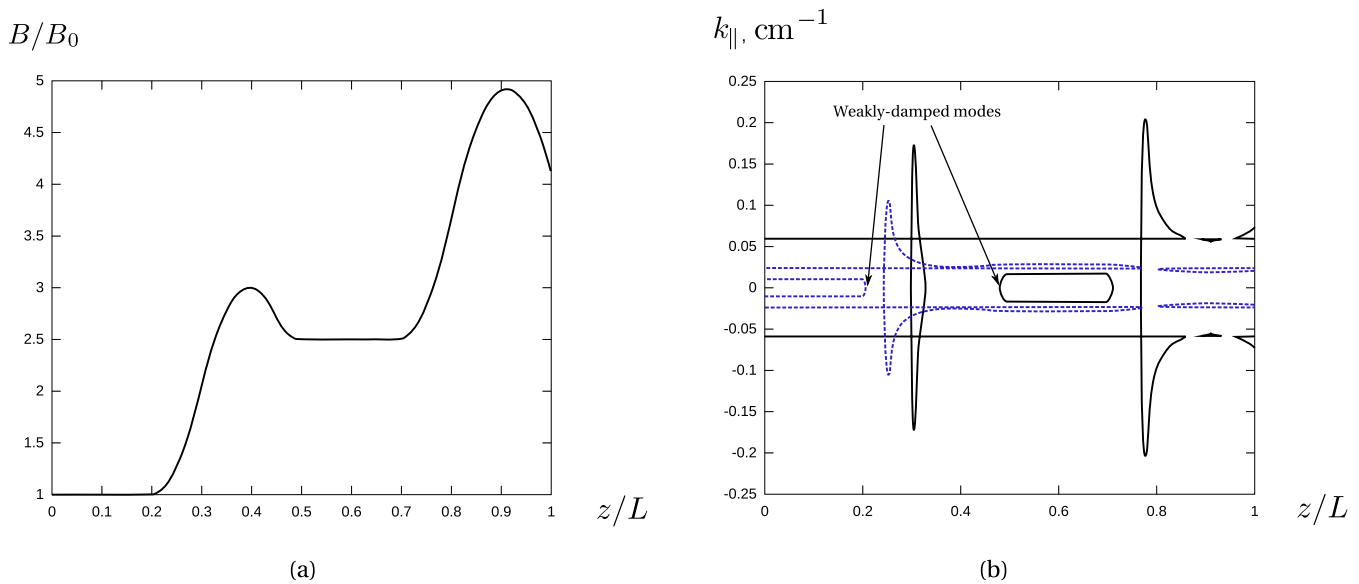


FIG. 7. (Color online) (a) The magnetic field profile in a system with three magnetic field wells. One well is near the midplane at  $z=0$  and the other two are at  $|z|=z_m \approx 0.6L$ . (b) The dependence  $k_{||}(z/L)$  for two waves with  $\omega_1 \approx 0.8\Omega_D^0$  (dashed) and  $\omega_2 \approx 2\Omega_D^0$  (solid), where  $\Omega_D^0$  is a deuterium gyrofrequency at the midplane. Three weakly damped modes located near  $z=0$  and  $|z|=z_m$  are indicated with arrows.

described by Eq. (12) for  $\alpha$ -channeling at an arbitrary axial position, a magnetic field profile with several minimum- $B$  wells can be employed. For example, the  $k_{||}(\eta)$  dependencies for two waves with equal values of  $k_{\perp}$ , but different values of  $\omega$  with the magnetic field profile illustrated in Fig. 7(a), is shown in Fig. 7(b). Three weakly damped ion-cyclotron modes, one at the midplane, and others at  $|z|=z_m$ , exist in such a configuration and are shown in Fig. 7(b) with arrows.

#### IV. DISCUSSION

We described the limitations on the wave parameters necessary to achieve a high  $\alpha$ -channeling efficiency. In particular, ion-cyclotron waves weakly damped on electrons and having  $k_{||} \ll k_{\perp}$ ,  $k_{\perp} \rho_{\alpha} \geq 1$  are considered suitable for  $\alpha$ -channeling. Assuming that such waves propagate either along the magnetic field lines, or perpendicular to them, we proposed an algorithm to identify modes with desired properties in a given mirror machine configuration. In order to find weakly damped modes, we both (i) looked for waves with  $k_{||} \approx 0$  and (ii) analyzed the dependence of  $k_{||}$  on  $B$ , looking for closed loops, or half of closed loops, located away from regions subjected to strong Landau or ion cyclotron damping. This method was applied to two mirror machine designs: a proof-of-principle facility and a fusion reactor prototype.

As a result, we were able to identify mode candidates suitable for  $\alpha$ -channeling in both devices. By simulating a two-dimensional ray trajectory, we confirmed the validity of the method and showed that there exist weakly damped fast waves localized both radially and axially for which  $k_{||}$  is always smaller than any pre-chosen value. These modes were shown to interact with deeply trapped  $\alpha$  particles, while being weakly damped on electrons and even more weakly damped on ions. Furthermore, in order to improve prospects of the weakly damped mode excitation for  $\alpha$ -channeling in

mirror machines, a possibility to arrange several rf regions at different axial positions using magnetic field profile with several wells was demonstrated.

The fact that modes suitable for  $\alpha$ -channeling exist does not yet mean that a complete scenario has been demonstrated. It does remain to determine the fraction of affected  $\alpha$  particles and the expected  $\alpha$ -channeling efficiency. Furthermore, the methods used here to find waves suitable for  $\alpha$ -channeling do not exhaust all possibilities. Moreover, the plasma configuration considered is simple; more complicated configurations of plasma may permit other wave candidates. Thus, while an extensive search of suitable waves was conducted here, other candidate modes, possibly superior to the ones identified here, may in fact exist, and remain to be discovered.

#### ACKNOWLEDGMENTS

This work was supported by DOE Contracts No. DE-FG02-06ER54851 and DE-AC0276-CH03073.

#### APPENDIX: RESTRICTIONS ON WAVE PARAMETERS

The  $\alpha$ -channeling effect occurs in the phase space  $(\mathbf{r}, \mathbf{p})$ , such that  $\alpha$  particles born through fusion reactions then diffuse along one-dimensional paths due to resonant interaction with electromagnetic waves. If the diffusion induced along the path is suppressed at high energy, whereas at low-energy there is an effective particle “sink,” the interaction with the waves will result in the ejection of the cold  $\alpha$  particles from the system and the simultaneous transfer of their initial energy to the waves, thereby accomplishing the so-called  $\alpha$ -channeling effect. The  $\alpha$  particle ejection leads to fusion ash removal, while by coupling the amplified wave to ion species, it is possible to redirect extracted energy to fuel ions,

thus increasing the effective fusion reactivity compared with the typical scenario, in which  $\alpha$  particles heat plasma by slowing down collisionally on electrons.

Considering the wave- $\alpha$  particle interaction and the wave damping on ions and electrons independently, we will now derive the limitations on the wave parameters necessary to maximize the energy transfer from  $\alpha$  particles to fuel ions. In particular, we show that weakly damped electromagnetic waves in the ion-cyclotron frequency range with  $k_{\parallel} \ll k_{\perp}$ ,  $k_{\perp} \rho_{\alpha} \geq 1$ , and with damping on electrons weaker than damping on ions, are suitable for  $\alpha$ -channeling.

## 1. Diffusion path shape

The diffusion path can be seen from the Hamiltonian of a particle moving in a homogeneous background magnetic field and a plane wave, which can be written as

$$H = \frac{(\mathbf{p} - q\mathbf{A}_0/c - q\mathbf{A}_{\sim}/c)^2}{2M} + q\varphi_{\sim}, \quad (\text{A1})$$

where  $q$  and  $M$  are the particle charge and mass, correspondingly,  $\varphi_{\sim}$  and  $\mathbf{A}_{\sim}$  are scalar and vector potentials of the electromagnetic wave, and  $\mathbf{A}_0$  is a vector potential of the background dc magnetic field  $\mathbf{B} = \hat{z}B$  with  $\hat{z}$  being a unit vector directed along the  $z$  axis.

First we derive the resonance condition. Assuming that the wave field is weak, one can find the particle trajectory using Hamiltonian perturbation theory,<sup>38</sup> treating terms proportional to  $\mathbf{A}_{\sim}$  and  $\varphi_{\sim}$  as weak perturbations to the unperturbed Hamiltonian  $H_0 = (\mathbf{p} - q\mathbf{A}_0/c)^2/(2M)$ . According to KAM theorem,<sup>38</sup> the invariant tori of the unperturbed problem located near the resonances  $\omega - n\Omega - k_z v_z = 0$  are destroyed, where  $\omega$  is a wave frequency,  $\Omega$  is a cyclotron frequency,  $\mathbf{k}$  is a wave vector,  $\mathbf{v}$  is a particle velocity, and  $n$  is an arbitrary integer number. Fixing  $\Omega$ ,  $n$  and  $\alpha$  particle parallel resonant velocity  $v_z^0$ , the resonance condition can be understood as a relation between the required  $\omega$  and  $k_z$ .

The shape of the diffusion path can be derived from Eq. (A1). Since  $\varphi_{\sim}$  and  $\mathbf{A}_{\sim}$  depend on time through the wave phase  $\omega t - \mathbf{k}\mathbf{r}$ , as a result of a canonical transformation to a new longitudinal coordinate  $\kappa = z - \omega t/k_z$ , the new Hamiltonian  $\mathcal{H}$  will be independent of time and will take the form

$$\mathcal{H} = \frac{(\mathbf{P} - q\mathbf{A}(x, y, \kappa)/c)^2}{2M} + q\varphi(x, y, \kappa) - P_z \omega/k_z,$$

where  $\mathbf{A} = \mathbf{A}_0 + \mathbf{A}_{\sim}$ ,  $\mathbf{P}$  is a new canonical momentum, and  $\kappa$  is a new longitudinal canonical coordinate. Introducing the kinetic particle momentum  $\mathbf{p} = M\dot{\mathbf{r}}$ , and using  $A_{0z} = 0$ , the conservation of  $\mathcal{H}$  leads to

$$\frac{p_{\perp}^2}{2M} + \frac{(p_z - M\omega/k_z)^2}{2M} + q\varphi - \frac{q\omega}{ck_z} A_{\sim z} = \text{const},$$

where  $p_{\perp}^2 = p_x^2 + p_y^2$ . Therefore, a particle resonantly interacting with the wave diffuses along a one-dimensional path defined by the equation  $p_{\perp}^2 + (p_z - M\omega/k_z)^2 = \text{const}$  describing a circle in  $(p_{\perp}, p_z)$  space. To keep the wave in resonance with the particle while it moves along the path, the particle parallel velocity should remain nearly constant, which will be achieved when  $k_z v_{\perp} \ll \omega$ . If the further condition

$k_{\perp} \rho_{\alpha} = \rho_{\alpha} \sqrt{k_x^2 + k_y^2} \geq 1$  is also satisfied, this limitation can be rewritten as  $k_z \ll nk_{\perp}$ . Note, however, that if  $k_z \geq nk_{\perp}$  and  $k_z$  depends on  $z$ , then the diffusion of a particle repeatedly interacting with a wave will be accompanied by a change of  $v_z$  and thus a change of the position where the resonance condition  $\omega - n\Omega - k_z v_z = 0$  is satisfied. This effect, accompanied by a proper choice of the wave longitudinal profile, might be a useful tool for manipulating particle diffusion along the path, but is not pursued in this work.

## 2. Suppression of the diffusion along the path

A limitation on  $k_{\perp}$  value follows from the analysis of the particle diffusion. The quasilinear diffusion equation written along the resonant path for a homogeneous magnetic field can be written as<sup>39</sup>

$$\frac{\partial p}{\partial t} = \frac{\partial}{\partial l} \left( D_l \frac{\partial p}{\partial l} \right), \quad (\text{A2})$$

where  $D_l$  is a diffusion coefficient,  $l$  is a linear coordinate along the diffusion path in the multi-dimensional action variable space of the unperturbed problem and  $p(l; t)$  is a particle density on the path. The action variables of the unperturbed problem are the parallel momentum  $p_{\parallel}$ , the magnetic moment  $\mu = mv_{\perp}^2/2B$ , negative particle energy  $-H$ , and  $m\Omega X$ , where  $X$  is an  $x$  component of the particle guiding center.<sup>40,41</sup> Notice that if at some point  $l = l_0$ ,  $D_l(l)$  vanishes, particles cannot diffuse past such a point.<sup>42</sup> This effect is particularly important for limiting  $\alpha$  particle heating and hence reducing average  $\alpha$  particle extraction time. The optimal value of  $l_0$  should be greater than  $l = l_b$ , where  $\alpha$  particles are born, but it cannot be much greater than  $l_b$  either, because this would result in heating of particles. If there is only one wave resonant with a given  $\alpha$  particle, the condition  $l_0 \geq l_b$  limits  $k_{\perp} \rho_{\alpha}(l_b)$ . For example, for an electrostatic wave,  $D_E \sim J_n^2(k_{\perp} \rho_{\alpha})$ , where  $D_E$  is a characteristic energy-space diffusion coefficient and  $J_n$  is the Bessel function of order  $n$ . This suggests that  $k_{\perp} \rho_{\alpha}(l_b)$  should be somewhat less than the first positive zero of the Bessel function  $J_n(x)$ .

If there are several uncorrelated waves with identical  $k_z$  and  $\omega$ , but different transverse wave numbers  $k_{\perp i}$ , the diffusion along the path is not suppressed by previously discussed effects, but it can be avoided by the radial limitation of the wave. If for every  $i$  and  $j$ , one has  $|k_{\perp i} - k_{\perp j}| \ll k_{\perp i}$ , finite excursion of the particle energy  $\Delta E$  leads to a particle radial excursion  $\Delta r \sim -k_{\perp} \Delta E (m_{\alpha} \omega \Omega)^{-1} \sim -k_{\perp} \rho_{\alpha}^2/n$ , where  $m_{\alpha}$  is the  $\alpha$  particle mass, and  $k_{\perp}$  is an average of  $k_{\perp i}$ . Thus, by choosing  $k_{\perp} \rho_{\alpha}(l_b) \gg 1$ , which allows radial displacements much larger than  $\rho$ , and by limiting radial wave profile,  $\alpha$  particle heating is constrained by the maximum possible radial excursion before the particle leaves the wave.

## 3. Required wave damping rates

Efficient  $\alpha$ -channeling is possible only if the wave amplitude is much larger than a certain critical value  $f_0$  at which the characteristic  $\alpha$  particle extraction time  $\tau_{\text{extr}}$  is of order of the typical collisional  $\alpha$ -electron energy relaxation time  $\tau_{ae}$ . But even if  $\tau_{\text{extr}} \gg \tau_{ae}$ , electrons can gain more energy than

ions if the wave damping on electrons is stronger than the wave damping on ions. Therefore, we will further focus our attention on waves with  $\tau_e \gg \tau_i$ , where  $\tau_s$  is a characteristic Landau or ion-cyclotron wave damping time on species  $s$ . If for some wave  $\tau_i \geq \tau_e$ , we will assume that there exist another mechanism which can transport wave energy to ions on the characteristic time scale further denoted by the same  $\tau_i$ , which is much smaller than  $\tau_e$ .

Another limitation on  $\tau_i$  follows from the fact that the  $\alpha$ -channeling technique is practical only if the energy extracted from  $\alpha$  particles exceeds the energy necessary to excite the channeling wave. Assuming that the geometrical optics approximation is valid, one can consider two wave launching schemes: (a) excitation of a weakly damped mode trapped in the device core, and (b) excitation of a traveling wave which first extracts energy from  $\alpha$  particles and then dissipates it on ions. The choice of a particular scheme depends on a dimensionless parameter  $\xi = \tau_{\text{amp}} / \tau_L$ , where  $\tau_L$  is the time it takes the wave packet to travel a distance comparable to the device length  $L$  and  $\tau_{\text{amp}}$  is the characteristic wave amplification time. If the rate of  $\alpha$  particle production is so large that  $\xi \ll 1$ , then  $\alpha$ -channeling can be implemented by launching a traveling wave. If, in turn,  $\xi \gg 1$ , then the excitation of a weakly damped mode is necessary. If for such a weakly damped mode,  $\tau_i$  is smaller than the characteristic wave energy amplification time  $\tau_{\text{amp}}$  and  $\tau_{\text{amp}} - \tau_i \ll \tau_i$ , the wave energy will decrease, but slowly enough to extract much more  $\alpha$  particle energy than the energy necessary to excite the channeling wave. It is the latter case that is considered in this work.

<sup>1</sup>T. Intrator, S. Meassick, J. Browning, R. Majeski, J. R. Ferron, and N. Hershkovitz, *Nucl. Fusion* **29**, 377 (1989).

<sup>2</sup>Y. Amagishi, A. Tsushima, and M. Inutake, *Phys. Rev. Lett.* **48**, 1183 (1982).

<sup>3</sup>Y. Yamaguchi, M. Ichimura, H. Higaki, S. Kakimoto, K. Nakagome, K. Nemoto, M. Katano, H. Nakajima, A. Fukuyama, and T. Cho, *Plasma Phys. Controlled Fusion* **48**, 1155 (2006).

<sup>4</sup>Y. Yasaka, H. Takeno, A. Fukuyama, T. Toyoda, M. Miyakita, and R. Itatani, *Phys. Fluids B* **4**, 1486 (1992).

<sup>5</sup>Y. Yamaguchi, M. Ichimura, H. Higaki, S. Kakimoto, K. Horinouchi, K. Ide, D. Inoue, K. Nakagome, and A. Fukuyama, *J. Plasma Fusion Res.* **6**, 665 (2004).

<sup>6</sup>K. Yatsu, T. D. Akhmetov, T. Cho, M. Hirata, H. Hojo, M. Ichimura, K. Ishii, A. Itakura, Y. Ishimoto, I. Katanuma, J. Kohagura, Y. Nakashima, T. Saito, Y. Tatematsu, and M. Yoshikawa, *Proceedings of the 28th EPS Conference on Controlled Fusion and Plasma Physics*, Funchal, Portugal, 2001 (The European Physical Society, Geneva, 2001), Vol. 25A, p. 1549.

<sup>7</sup>R. I. Pinsky, *Phys. Plasmas* **8**, 1219 (2001).

<sup>8</sup>R. W. Clark, D. G. Swanson, P. Korn, F. Sandel, S. Robertson, and C. B. Wharton, *Phys. Fluids* **17**, 1322 (1974).

<sup>9</sup>W. C. Turner, *J. Phys. Colloq.* **38**, C6-121 (1977).

<sup>10</sup>R. Majeski, J. J. Browning, S. Meassick, N. Hershkovitz, T. Intrator, and J. R. Ferron, *Phys. Rev. Lett.* **59**, 206 (1987).

<sup>11</sup>H. Jhang, S. G. Lee, S. S. Kim, B. H. Park, and J. G. Bak, *Phys. Rev. Lett.* **95**, 035005 (2005).

<sup>12</sup>J. Kesner, *Nucl. Fusion* **19**, 108 (1979).

<sup>13</sup>R. Breun, S. N. Golovato, L. Yujiri, B. McVey, A. Molvik, D. Smatlak, R. S. Post, D. K. Smith, and N. Hershkovitz, *Phys. Rev. Lett.* **47**, 1833 (1981).

<sup>14</sup>C. Riccardi, M. Fontanesi, A. Galassi, and E. Sindoni, *Il Nuovo Cimento D* **16**, 505 (1994).

<sup>15</sup>H. Sugai, H. Kojima, and T. Okuda, *Phys. Lett. A* **92**, 392 (1982).

<sup>16</sup>G. A. Wurden, M. Ono, and K. L. Wong, *Phys. Rev. A* **26**, 2297 (1982).

<sup>17</sup>C. Riccardi, P. Cantu, and M. Fontanesi, *Plasma Phys. Controlled Fusion* **37**, 885 (1995).

<sup>18</sup>N. J. Fisch and J. M. Rax, *Phys. Rev. Lett.* **69**, 612 (1992).

<sup>19</sup>N. J. Fisch, *Rev. Mod. Phys.* **59**, 175 (1987).

<sup>20</sup>N. J. Fisch and M. C. Herrmann, *Nucl. Fusion* **34**, 1541 (1994).

<sup>21</sup>N. J. Fisch, *Phys. Plasmas* **2**, 2375 (1995).

<sup>22</sup>N. J. Fisch and M. C. Herrmann, *Nucl. Fusion* **35**, 1753 (1995).

<sup>23</sup>M. C. Herrmann and N. J. Fisch, *Phys. Rev. Lett.* **79**, 1495 (1997).

<sup>24</sup>N. J. Fisch, *Phys. Rev. Lett.* **97**, 225001 (2006).

<sup>25</sup>N. J. Fisch, *Fusion Sci. Technol.* **51**, 1 (2007).

<sup>26</sup>A. J. Fetterman and N. J. Fisch, *Phys. Rev. Lett.* **101**, 205003 (2008).

<sup>27</sup>T. K. Fowler and M. Rankin, *J. Nucl. Energy Part C* **8**, 121 (1966).

<sup>28</sup>D. A. Gates, N. N. Gorelenkov, and R. B. White, *Phys. Rev. Lett.* **87**, 205003 (2001).

<sup>29</sup>R. G. L. Vann, H. L. Berk, and A. R. Soto-Chavez, *Phys. Rev. Lett.* **99**, 025003 (2007).

<sup>30</sup>H. L. Berk, *Transp. Theory Stat. Phys.* **34**, 205 (2005).

<sup>31</sup>H. L. Berk, C. J. Boswell, D. Borba, A. C. A. Figueiredo, T. Johnson, M. F. F. Nave, S. D. Pinches, and S. E. Sharapov, *Nucl. Fusion* **46**, S888 (2006).

<sup>32</sup>S. D. Pinches, H. L. Berk, D. N. Borba, B. N. Breizman, S. Briguglio, A. Fasoli, G. Fogaccia, M. P. Gryaznevich, V. Kiptily, M. J. Mantsinen, S. E. Sharapov, D. Testa, R. G. L. Vann, G. Vlad, F. Zonca, and JET-EFDA Contributors, *Plasma Phys. Controlled Fusion* **46**, B187 (2004).

<sup>33</sup>A. I. Zhmoginov and N. J. Fisch, *Phys. Plasmas* **15**, 042506 (2008).

<sup>34</sup>E. J. Valeo and N. J. Fisch, *Phys. Rev. Lett.* **73**, 3536 (1994).

<sup>35</sup>T. H. Stix, *Waves in Plasmas* (Springer-Verlag, Berlin, 1992).

<sup>36</sup>J. Pratt and W. Horton, *Phys. Plasmas* **13**, 042513 (2006).

<sup>37</sup>J. Pratt, W. Horton, and H. L. Berk, *J. Fusion Energy* **27**, 91 (2008).

<sup>38</sup>A. J. Lichtenberg and M. A. Leiberman, *Regular and Chaotic Dynamics* (Springer-Verlag, Berlin, 1992).

<sup>39</sup>G. R. Smith and B. I. Cohen, *Phys. Fluids* **26**, 238 (1983).

<sup>40</sup>G. R. Smith and A. N. Kaufman, *Phys. Fluids* **21**, 2230 (1978).

<sup>41</sup>C. F. F. Karney, *Phys. Fluids* **22**, 2188 (1979).

<sup>42</sup>Y. Kiyamoto, H. Abe, T. Aota, L. G. Bruskin, T. Cho, T. Goto, M. Hirata, H. Hojo, M. Ichimura, K. Ikeda, K. Ishii, A. Itakura, K. Kajiwara, I. Katanuma, N. Katsuragawa, I. M. Khairul, J. Kohagura, A. Kumagai, A. Mase, Y. Nagayama, Y. Nakashima, N. Oyama, T. Saito, Y. Sakamoto, M. Shoji, T. Takahashi, T. Tamano, S. Tanaka, Y. Tatematsu, T. Tokuzawa, N. Yamaguchi, K. Yatsu, M. Yoshikawa, and Y. Yoshimura, *Plasma Phys. Controlled Fusion* **39**, A381 (1997).